

Spectral modeling of magnetohydrodynamic turbulent flows

J. Baerenzung

TNT/NCAR, P.O. Box 3000, Boulder, Colorado 80307-3000, USA

and Observatoire de la Côte d'Azur, Université de Nice–Sophia Antipolis, CNRS UMR 6202, Boîte Postale 4229, 06304 Nice Cedex 4, France

H. Politano and Y. Ponty

Observatoire de la Côte d'Azur, Université de Nice–Sophia Antipolis, CNRS UMR 6202, Boîte Postale 4229, 06304 Nice Cedex 4, France

A. Pouquet

TNT/NCAR, P.O. Box 3000, Boulder, Colorado 80307-3000, USA

(Received 24 March 2008; published 29 August 2008)

We present a dynamical spectral model for large-eddy simulation of the incompressible magnetohydrodynamic (MHD) equations based on the eddy damped quasinormal Markovian approximation. This model extends classical spectral large-eddy simulations for the Navier-Stokes equations to incorporate general (non-Kolmogorovian) spectra as well as eddy noise. We derive the model for MHD flows and show that the introduction of an eddy damping time for the dynamics of spectral tensors, in the absence of equipartition between the velocity and magnetic fields, leads to better agreement with direct numerical simulations, an important point for dynamo computations.

DOI: [10.1103/PhysRevE.78.026310](https://doi.org/10.1103/PhysRevE.78.026310)

PACS number(s): 47.27.E–, 47.27.em, 47.65.–d, 47.11.Kb

I. INTRODUCTION

Magnetic fields permeate the universe. For example, electric fields and ionospheric currents play a dynamic role in the evolution of the atmosphere above 100 km, and the input of energy from the magnetosphere during magnetic storms can affect the thermosphere and ionosphere on global scales. If kinetic effects—such as the Hall current, ambipolar drift, or anisotropic pressure tensor—may be prevalent at small scales, the large scales can be described by means of the magnetohydrodynamic (MHD) approximation.

MHD turbulence shares many similarities with Navier-Stokes turbulence: recall the Batchelor analogy between vorticity and induction, both undergoing stretching through velocity gradients [see Eq. (6)]. On that basis, one can conjecture that the energy spectrum in MHD will be of the Kolmogorov type, as in fact observed in numerical simulations of decaying flows ([1] and references therein), as well as in the solar wind [2]. However, Iroshnikov and Kraichnan (IK) hypothesized that the slowing down of nonlinear transfer by Alfvén waves would alter the energy spectrum behavior [3], predicting a spectrum $\sim k^{-3/2}$, as recently observed in numerical simulations [4–6] and in solar wind observations [7]. The Lagrangian renormalized approximation also provides spectra compatible with the IK phenomenology [8]. These one-dimensional spectra are based on the assumption of homogeneity and isotropy, but the presence of a strong quasiuniform magnetic field \mathbf{B}_0 at large scale leads to an anisotropic dynamics. One can evaluate exactly the reduced dynamics in that case [9], using weak turbulence theory; the emerging energy spectrum scales as \mathbf{k}_\perp^{-2} , where \mathbf{k}_\perp refers to wave vectors perpendicular to the \mathbf{B}_0 direction (the isotropization of such a spectrum being compatible with the IK spectrum); a weak turbulence spectrum was in fact deduced from an analysis of Galileo spacecraft data collected in the Jovian magnetosphere [10]. Such a spectrum was also ob-

served in a large numerical simulation of the MHD equations in three dimensions in the absence of forcing, at a magnetic Taylor Reynolds number of ~ 1700 , at scales smaller than the magnetic Taylor scale [6].

Both the terrestrial and Jovian magnetospheric plasmas, as well as the solar wind, the solar atmosphere, or the interstellar medium (ISM) are highly turbulent conducting compressible flows sustaining magneto-acoustic wave propagation; a better understanding of their dynamics, leading, for example, to coronal mass ejection from the sun, or to star formation in the ISM, requires adequate tools to model them. Furthermore, there is currently a surge of interest in achieving experimental dynamos (the growth of a seed magnetic field through fluid motions; see [11]). In liquid metals, in the fluid core of the Earth [12–14], as well as in the solar convection zone, the magnetic Prandtl number P_M (the ratio of viscosity to magnetic resistivity) is very small (10^{-5} or less); hence, the dynamo instability occurs within a turbulent flow. To tackle this problem from a numerical standpoint, one can resort to modeling the kinetic turbulent fluctuations only, leaving the induction equation unchanged [15,16]. However, this approach cannot be applied when the magnetic field intensity is of the order of, or larger than, the velocity, the interactions between these two fields being sizable. The main difficulty when attempting to model these interactions comes from the fact that the energy transfer between the small-scale flow and the large-scale flow can be important, such interactions being measurably nonlocal [17–19]. Until now, only a few models for MHD turbulence have been studied (see, e.g., [20] for a model in physical space, and the recent review in [21] for models in spectral space), when compared to the fluid case, where modeling is a very active field of research, e.g., in the engineering community.

In this context, the present paper aims at developing a spectral large-eddy simulation (LES) model, following the work of Chollet and Lesieur [22] for the Navier-Stokes equa-

tions, and making use of existing two-point closures for MHD flows (see, e.g., [23] for a review). The basic MHD equations are given in the next section. The closure formulation of the eddy damped quasinormal approximation (EDQNM) for MHD turbulence is recalled in Sec. III (with a related technical part given in the Appendix). Numerical tests of a first model (LES MHD I) are performed and lead us to reexamine the eddy damping time used in the original closure [24,25]. Triad relaxation times are thus introduced in Sec. IV and a second model (LES MHD II) is derived. Section V describes the numerical setup we use to study freely decaying flows and test the two MHD models. The case of random flows at two different magnetic Prandtl numbers is treated, respectively, in Secs. VI (with $P_M=1$) and VIII ($P_M=0.1$), while the case of deterministic initial conditions, namely, the so-called three-dimensional Orszag-Tang flow, at $P_M=1$, is analyzed in Sec. VIII. Finally, Sec. IX is the conclusion.

II. MAGNETOHYDRODYNAMIC EQUATIONS

The MHD equations describe the time evolution of a conducting fluid, with velocity $\mathbf{v}(\mathbf{x},t)$ and magnetic field $\mathbf{B}(\mathbf{x},t)$ coupled through the Lorentz force $\mathbf{j} \times \mathbf{B}$, with $\mathbf{j} = \nabla \times \mathbf{B}$. These equations derive from Maxwell's equations, assuming subrelativistic velocities; hence the displacement current is neglected [26,27]. Considering the Fourier transform of the velocity and the magnetic field at wave vector \mathbf{k} ,

$$\mathbf{v}(\mathbf{k},t) = \int_{-\infty}^{\infty} \int_{-\infty}^{\infty} \int_{-\infty}^{\infty} \mathbf{v}(\mathbf{x},t) e^{-i\mathbf{k} \cdot \mathbf{x}} d\mathbf{x}, \quad (1)$$

$$\mathbf{B}(\mathbf{k},t) = \int_{-\infty}^{\infty} \int_{-\infty}^{\infty} \int_{-\infty}^{\infty} \mathbf{B}(\mathbf{x},t) e^{-i\mathbf{k} \cdot \mathbf{x}} d\mathbf{x}, \quad (2)$$

the MHD equations can be written in terms of the velocity and magnetic Fourier coefficients

$$\left(\frac{\partial}{\partial t} + \nu k^2 \right) \mathbf{v}(\mathbf{k},t) = \mathbf{t}^V(\mathbf{k},t), \quad (3)$$

$$\left(\frac{\partial}{\partial t} + \eta k^2 \right) \mathbf{b}(\mathbf{k},t) = \mathbf{t}^M(\mathbf{k},t), \quad (4)$$

together with the incompressibility conditions $\mathbf{k} \cdot \mathbf{v} = 0$ and $\mathbf{k} \cdot \mathbf{b} = 0$ (indicating the lack of magnetic monopoles in the classical approximation), and assuming a constant unit density $\rho_0 \equiv 1$. Here, $\mathbf{b} = \mathbf{B} / \sqrt{\mu_0 \rho_0}$ is the Alfvén velocity, with μ_0 the permeability; η is the magnetic diffusivity, ν is the kinematic viscosity, and $\mathbf{t}^V(\mathbf{k},t)$ and $\mathbf{t}^M(\mathbf{k},t)$ are bilinear operators for the kinetic and magnetic energy transfers, written as

$$\begin{aligned} t_\alpha^V(\mathbf{k},t) = & -i P_{\alpha\beta}(\mathbf{k}) k_\gamma \sum_{\mathbf{p}+\mathbf{q}=\mathbf{k}} v_\beta(\mathbf{p},t) v_\gamma(\mathbf{q},t) \\ & + i P_{\alpha\beta}(\mathbf{k}) k_\gamma \sum_{\mathbf{p}+\mathbf{q}=\mathbf{k}} b_\beta(\mathbf{p},t) b_\gamma(\mathbf{q},t), \end{aligned} \quad (5)$$

$$\begin{aligned} t_\alpha^M(\mathbf{k},t) = & -i \delta_{\alpha\beta} k_\gamma \sum_{\mathbf{p}+\mathbf{q}=\mathbf{k}} b_\beta(\mathbf{p},t) v_\gamma(\mathbf{q},t) \\ & - i \delta_{\alpha\beta} k_\gamma \sum_{\mathbf{p}+\mathbf{q}=\mathbf{k}} b_\beta(\mathbf{q},t) v_\gamma(\mathbf{p},t), \end{aligned} \quad (6)$$

where $P_{\alpha\beta}(\mathbf{k}) = \delta_{\alpha\beta} - k_\alpha k_\beta / k^2$ is a projector that allows us to take the pressure term of the velocity equation into account via a Poisson formulation. The magnetic Prandtl number is defined as $P_M = \nu / \eta$. Finally, note that the total energy $E_T = 0.5(\mathbf{v}^2 + \mathbf{b}^2)$, the cross correlation (or cross helicity) between the kinetic and magnetic fluctuations, $H_C = \langle \mathbf{v} \cdot \mathbf{b} \rangle$, and the magnetic helicity $\langle \mathbf{A} \cdot \mathbf{b} \rangle$ (with $\mathbf{b} = \nabla \times \mathbf{A}$) are invariants of the three-dimensional MHD equations in the ideal case, i.e., in the absence of viscous and resistive dissipation ($\nu = 0 = \eta$).

III. SPECTRAL MODELING

A. The original EDQNM closure for MHD

The large-eddy simulation model derived in [28] for Navier-Stokes flows (paper I hereafter) is now extended to the MHD equations in its nonhelical version (LES-P, where ‘‘P’’ stands for ‘‘partial phase’’), i.e., intrinsic variations of the helicity spectra are not taken into account. In a first step, a spectral filtering of the equations is realized; this operation consists in truncating all velocity and magnetic components at wave vectors \mathbf{k} such that $|\mathbf{k}| = k > k_c$, where k_c is a so-called cutoff wave number. Since the scales associated with k_c are presumably much larger than the actual dissipative small scales in a high-Reynolds-number flow, one needs to model the transfer between the large (resolved) scales and the small (subgrid, unresolved) scales of the flow. In order to approximate these transfer terms, the behavior of the energy spectra after the cutoff wave number has to be estimated. We therefore define an intermediate range, lying between k_c and $3k_c$, where both kinetic and magnetic energy spectra are assumed to present a power-law behavior followed by an exponential decrease:

$$E^V(k,t) = E_0^V k^{-\alpha_V^V} e^{-\delta_E^V k}, \quad k_c \leq k < 3k_c, \quad (7)$$

$$E^M(k,t) = E_0^M k^{-\alpha_E^M} e^{-\delta_E^M k}, \quad k_c \leq k < 3k_c. \quad (8)$$

The coefficients $\alpha_E^{V,M}$, $\delta_E^{V,M}$, and $E_0^{V,M}$ are computed at each time step, through a mean-square fit of the resolved kinetic and magnetic energy spectra. In a second step, one can write the following modeled MHD equations:

$$[\partial_t + (\nu(k|k_c,t) + \nu k^2)] v_\alpha(\mathbf{k},t) = t_\alpha^{V<}(\mathbf{k},t), \quad (9)$$

$$\{\partial_t + [\eta(k|k_c,t) + \eta k^2]\} b_\alpha(\mathbf{k},t) = t_\alpha^{M<}(\mathbf{k},t), \quad (10)$$

where the $<$ symbol indicates that the nonlinear transfers are integrated over a truncated domain defined such as $\mathbf{p} + \mathbf{q} = \mathbf{k}$ with $|\mathbf{p}| = p$, $|\mathbf{q}| = q < k_c$. The $\nu(k|k_c,t)$ and $\eta(k|k_c,t)$ quantities, which are, respectively, called the eddy viscosity and the magnetic eddy diffusivity, are expressed as

$$\nu(k|k_c, t) = - \int \int_{\Delta^>} \theta_{kpq} \frac{[S_2^V(k, p, q, t) + S_4^V(k, p, q, t)]}{2k^2 E^V(k, t)} dp dq, \quad (11)$$

$$\eta(k|k_c, t) = - \int \int_{\Delta^>} \theta_{kpq} \frac{[S_2^M(k, p, q, t) + S_4^M(k, p, q, t)]}{2k^2 E^M(k, t)} dp dq \quad (12)$$

(see paper I for more details). Here, the $S_{2,4}^{V,M}(k, p, q, t)$ terms (see the Appendix), correspond to absorption terms [linear in the energy spectra $E^{V,M}(k, t)$] in the EDQNM nonlinear transfers, leading in particular to turbulent eddy diffusivities (see, e.g., [24,25] for the MHD case). $\Delta^>$ is the integration domain over $(\mathbf{k}, \mathbf{p}, \mathbf{q})$ triangles, such that p and/or q are larger than k_c , and both p and q are smaller than $3k_c$.

Finally, to take into account effects from the emission (eddy noise) terms involved in the EDQNM nonlinear transfers [i.e., $S_{1,3}^{V,M}(k, p, q, t)$], we use a reconstruction field procedure which also enables us to partly rebuild the phase relationships between the three spectral components of each velocity and magnetic fields, as explained in paper I [28].

B. First numerical tests

We first implemented our numerical MHD LES model (LES MHD I) using the initial EDQNM equations derived by Pouquet *et al.* [25] (see also [24] for the nonhelical case). In this formulation, the triad relaxation time Θ_{kpq} given in the Appendix is based on three characteristic times: a (combined) dissipation time τ_D defined as

$$\tau_D^{-1}(k) = (\nu + \eta)k^2, \quad (13)$$

a nonlinear time τ_S expressed as

$$\tau_S^{-1}(k) = \lambda \left(\int_0^k q^2 [E^V(q) + E^M(q)] dq \right)^{1/2}, \quad (14)$$

and an Alfvén time τ_A , which reads

$$\tau_A^{-1}(k) = \left(\frac{2}{3} \right)^{1/2} k \left(\int_0^k E^M(q) dq \right)^{1/2}. \quad (15)$$

This corresponds to a straightforward generalization of the fluid EDQNM closure to the case of MHD flows (see, for example, [23]), with two new times, specifically the Alfvén time built on large-scale magnetic energy and the diffusion time built on magnetic resistivity; both times are incorporated in a phenomenological manner. A comparison of a simulation using this LES MHD I model (run II in Table I), against a direct numerical simulation (DNS) (run I in Table I) is shown in Fig. 1 for random initial conditions (see the next section for a description of the chosen numerical procedure). One can see that both kinetic and magnetic energy spectra are overestimated by the model at scales close to the cutoff, which is indicative of an inadequate modeled energy transfer at these scales. When evaluating the different eddy damping times (13)–(15) from numerical data, one observes that the Alfvén time is almost one order of magnitude shorter than all

TABLE I. Parameters of the simulations. Initial conditions (IC) resolution N^3 , kinematic viscosity ν , and magnetic Prandtl number $P_M = \nu / \eta$, with η the magnetic diffusivity. All random flows have negligible correlation between the velocity and the magnetic field, whereas for the Orszag-Tang (OT) vortex, the normalized correlation is close to 0.4 at $t=0$.

		IC	N^3	ν	P_M
I	DNS	Random	256^3	2×10^{-3}	1
II	LES MHD I	Random	64^3	2×10^{-3}	1
III	LES MHD II	Random	64^3	2×10^{-3}	1
IV	DNS	Random	256^3	8×10^{-4}	0.1
V	LES MHD II	Random	64^3	8×10^{-4}	0.1
VI	LES MHD I	Random	64^3	8×10^{-4}	0.1
VII	DNS	OT	256^3	2×10^{-3}	1
VIII	LES MHD II	OT	64^3	2×10^{-3}	1

other times, including the diffusion time at the smallest resolved scales (see [29]); this leads to an insufficient damping at scales close to the cutoff. This is in part due to the prevalence of the magnetic energy at large scale, and, in that sense, it could be linked to the particular flow under study.

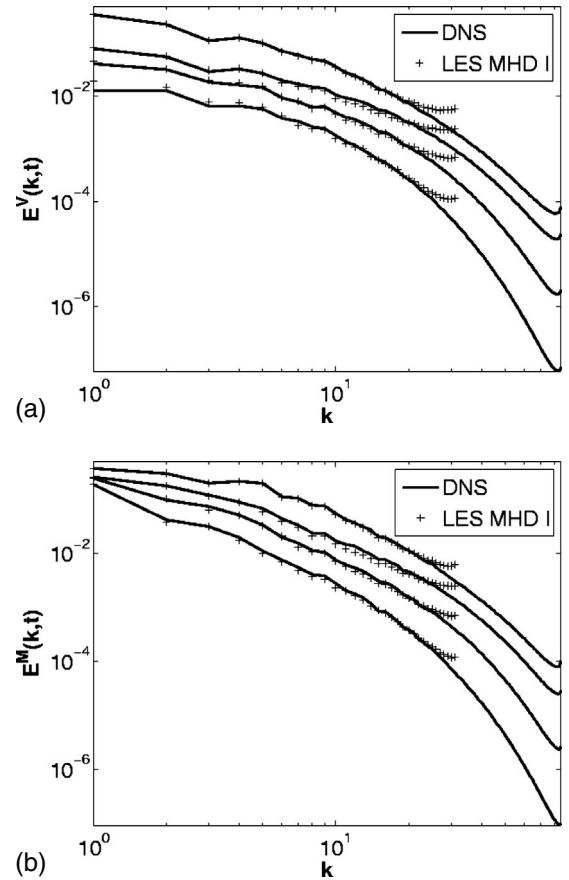


FIG. 1. Kinetic (top) and magnetic (bottom) energy spectra for data sets I (256^3 DNS, solid line), and II (64^3 LES MHD I, plus signs). Successive times ($t=1, 3, 5$, and 10) are plotted within each graph, from upper to lower curves. Note the overshoot of the LES spectra close to the cutoff wave number.

Hence, parametric analyses for several different flows should be performed in the future in order to fine-tune this MHD model. However, the discrepancy displayed in Fig. 1 could also be linked to the particular eddy damping time chosen in [25]. We are thus led to closely examine the energy transfer dynamics within the EDQNM closure framework.

IV. RELAXATION TIMES FOR EDQNM

We now analyze the precise structure of the equations leading to the MHD EDQNM closure in order to find new relaxation times. In [25], the eddy damping term is built on phenomenological grounds; namely, by arguing the case for considering the necessity to introduce the Alfvén time scale in the damping coefficient, actually without referring to the set of cumulant expansion equations. This one change, from the usual hydrodynamic EDQNM closure, leads to energy spectra that differ from the Kolmogorov type, with a $k^{-3/2}$ law in the absence of correlations between the velocity and magnetic field, and with an $E^\pm(k) \sim k^{-m^\pm}$ spectrum in the correlated case [1], with $m^+ + m^- = 3$. Here, $E^\pm(k)$ are the energy spectra of the $\mathbf{z}^\pm = \mathbf{v} \pm \mathbf{b}$ Elsässer variables.

However, when examining the hierarchy of higher-order moment equations, in the uncorrelated case for the sake of simplicity, a more complex structure emerges, which may help to model the MHD dynamics more accurately and thus find a numerical behavior closer to the DNS results shown in Fig. 1. In fact, four different groups of terms are involved in the closure equations. The first group corresponds to the pure fluid case and it can be symbolically written as

$$\left(\frac{\partial}{\partial t} + \nu(k^2 + p^2 + q^2) \right) \langle uuuu \rangle \approx k \langle uuuu \rangle. \quad (16)$$

This leads, as usual, to two characteristic times $\tau_D^{VV} = [\nu(k^2 + p^2 + q^2)]^{-1}$ and $\tau_{NL} = (ku)^{-1}$.

The schematic expression for the second group is

$$\left(\frac{\partial}{\partial t} + \nu k^2 + \eta(p^2 + q^2) \right) \langle uuuu \rangle \approx k \langle uuuu \rangle + k \langle bbuu \rangle. \quad (17)$$

Hence, two new times can be extracted under the hypothesis of strict linear relaxation of fourth-order cumulants in terms of triple correlations, a hypothesis at the root of the EDQNM closure (as well as the assumption of zero velocity-magnetic field correlations, i.e., full mirror symmetry, as stated before). In the simplest case, this leads to the introduction of a dissipative time $\tau_D^{VM} = [\nu k^2 + \eta(p^2 + q^2)]^{-1}$, and of a modified Alfvén time $\tilde{\tau}_A = u(kbb)^{-1}$. Note that the Alfvén time introduced in the preceding section, in agreement with the formulation of [25], is of a purely phenomenological nature, whereas the methodology adopted here is to examine more closely the structure of the equations involving all moments up to fourth order.

The third group type in closure terms reads

$$\left(\frac{\partial}{\partial t} + (\eta k^2 + \eta p^2 + \nu q^2) \right) \langle bbu \rangle \approx k \langle bbbb \rangle + k \langle bbuu \rangle, \quad (18)$$

and finally, the fourth group is of the form

$$\left(\frac{\partial}{\partial t} + (\eta k^2 + \nu p^2 + \eta q^2) \right) \langle bbu \rangle \approx k \langle bbbb \rangle + k \langle bbuu \rangle. \quad (19)$$

Similarly, characteristic dissipative times can be deduced from these two last groups: $\tau_D^{MM} = (\eta k^2 + \eta p^2 + \nu q^2)^{-1}$ and $\tau_D^{MV} = (\eta k^2 + \nu p^2 + \eta q^2)^{-1}$.

A careful examination of the cumulant equations thus leads us to consider several new characteristic times, distinguishing between magnetic and kinetic energy transfers, as well as between the different quantities entering these transfers.

Since the EDQNM equations describe the temporal evolution of the isotropic kinetic and magnetic energy spectra, the characteristic times involved (i.e., the times used in the closure) cannot be functions of the flow velocity or magnetic fields, but they have to depend on their respective energies. By means of dimensional analysis, Pouquet *et al.* [25] proposed the following expression for the nonlinear turnover time:

$$\tau_{NL}^{-1}(k) = \lambda \left(\int_0^k q^2 E^V(q) dq \right)^{1/2}, \quad (20)$$

where the constant λ is determined by relation (A7) (see the Appendix). A similar analysis for the modified Alfvén time $\tilde{\tau}_A = u(kbb)^{-1} = u/b(kb)^{-1}$ allows us to approximate the b/u quantity:

$$\frac{b}{u} \approx \left(\frac{\int_0^k E^M(q) dq}{\int_0^k E^V(q) dq} \right)^{1/2} \quad (21)$$

and the kb quantity

$$kb \approx \left(\int_0^k q^2 E^M(q) dq \right)^{1/2}, \quad (22)$$

to finally obtain the following expression for the modified Alfvén time:

$$\tilde{\tau}_A^{-1}(k) = C_A \left(\frac{\int_0^k E^M(q) dq}{\int_0^k E^V(q) dq} \right)^{1/2} \left(\int_0^k q^2 E^M(q) dq \right)^{1/2}, \quad (23)$$

where the constant C_A is estimated to be approximately 0.8 according to several fits done in comparing with direct numerical simulations. One can notice that this new time incorporates the lack of equipartition between kinetic and magnetic energies but reverts to the traditional Alfvén time for

equipartition. This phenomenon of a discrepancy between the average amplitudes of the velocity and the magnetic field is often observed, e.g., in the solar wind. It should alter the flow dynamics, as, for example, in the early (kinematic) phase of the dynamo problem. Also note that the way the dissipation coefficients are now taken into account may well affect the results as well when the magnetic Prandtl number substantially differs from unity, except possibly when both the kinetic and magnetic Reynolds numbers are very large, since in that case one expects the renormalized transport coefficients to be close in value [30].

Having defined all the above characteristic times, we can derive triad relaxation times; this allows us to implement a second LES spectral model for MHD flows (LES MHD II) which we now test against several direct numerical simulations.

V. NUMERICAL SETUP

In order to assess the ability of the model to reproduce the physics involved in MHD periodic flows, we performed direct numerical simulations of the three-dimensional MHD equations, in a $(2\pi)^3$ periodic box, at a resolution of 256^3 grid points, together with computations using our LES MHD models, but now at 64^3 grid points. This comparative study is based on three different simulations of freely decaying flows. To test our model in a simple configuration, we first simulated a flow with $P_M=1$, taking random initial conditions and no correlation between the velocity and the magnetic fields (run I for the DNS, run II for the LES MHD I model, and run III for the LES MHD II model, in Table I). The initial kinetic and magnetic energy spectra are chosen to be proportional to $k^2 e^{-2(k/k_0)^2}$, with $k_0=2$, and with $E^V(t=0)=E^M(t=0)=2$.

Since the eddy damping times we derived allow for a clear distinction between the kinematic viscosity and the magnetic diffusivity, we then ran the same flow at a different magnetic Prandtl number, namely, $P_M=0.1$ (run IV DNS, and run V LES MHD II in Table I). We recall that, in [25], the EDQNM closure is derived in the case of identically zero cross correlation between the velocity and magnetic field (both globally and mode by mode), but including the effect of kinetic and magnetic helicities (see [1,33] for the nonhelical case in the presence of cross correlation). However, in many flows, the cross correlation may not be neglected. Furthermore, it can be locally strong (in particular in the vicinity of vorticity and current sheets) even when its global value is close to zero [31,32]. We thus performed as well a simulation at $P_M=1$ for which the velocity and the magnetic field are significantly correlated, in order to see how our model may adapt to such a situation. We chose the so-called three-dimensional Orszag-Tang flow for which initially $H^C/E^T=0.4$ (see Sec. VIII) (run VI DNS and run VII LES MHD II in Table I).

From all these simulations, we studied global flow quantities such as the total, kinetic, and magnetic energies, as well as kinetic, magnetic, and cross helicities. We also analyzed the spectral behavior of these quantities.

VI. RANDOM FLOW AT $P_M=1$

We first investigate the model behavior for a flow with random initial conditions, presenting no cross correlation, and at a magnetic Prandtl number of unity.

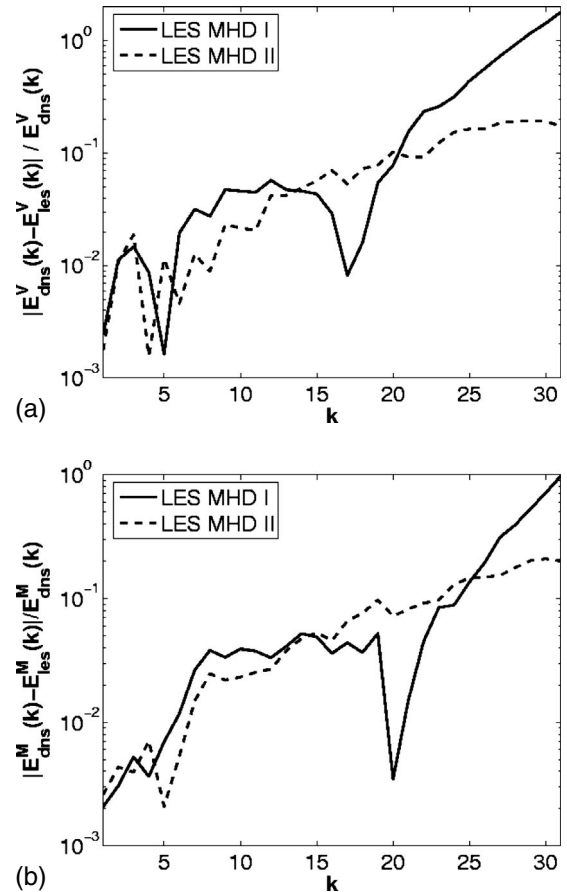


FIG. 2. Linear-log plots of the relative difference with DNS energy spectra for the velocity (top) and the magnetic field (bottom) at time $t=1$, for runs II and III, compared to the DNS, run I. Note that the large error in LES MHD I at large k , as already noted in Fig. 1, is substantially diminished in the current model.

A. Intercomparison of models

In this section, we compare the relative efficiency of the two models, namely, the model that involves the eddy damping times stemming from [25] (LES MHD I), and the model where the eddy damping times are now included (LES MHD II). In Fig. 2, we plot the relative difference between the kinetic and magnetic energy spectra computed from both LES models and those computed from the DNS data. The instantaneous spectra are chosen at time $t=1$, close to the time of maximum dissipation.

As already observed in Fig. 1, both kinetic and magnetic spectra predicted by the LES MHD I model exhibit a strong difference from the DNS spectra at small scales (between $k \approx 20-25$ and $k=31$). This effect, due to the underestimation of the energy transfer from large to small scales, is well cured by the LES MHD II model. One can also notice that at large scales (between $k=0$ and $k \approx 15$), where the effect of the modeling is weaker than at small scales, the LES model taking the eddy damping times into account also provides a closer estimation of the spectra than the initial model. Nevertheless, at intermediate scales ($k \approx 15$ and $k \approx 20-25$), the LES MHD I model seems to be more accurate than the LES MHD II model, but in fact this behavior is simply due to the

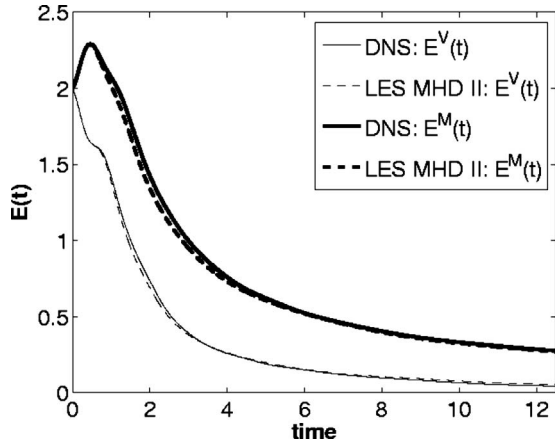


FIG. 3. Temporal evolution of the kinetic and magnetic energies for runs I (256^3 DNS) and III (64^3 LES MHD II).

fact that LES MHD I and DNS spectra cross at a wave number located inside these ranges. Although we do not show it in this paper, we realized the same analysis at different times in the simulation, and we always obtained similar results. We therefore mainly focus our study on the LES MHD II model for the remainder of the paper.

B. Global quantities

We now study the temporal evolution of the global kinetic, $E^V(t)$, and magnetic, $E^M(t)$, energies for runs I and III, as shown in Fig. 3. One can observe that the modeled kinetic and magnetic energies both closely follow the DNS evolution, although at moderate times [between $t=1$ and 5 for $E^M(t)$ and between $t=1$ and 3 for $E^V(t)$], the model slightly underestimates them.

Since our field reconstruction procedure uses the flow (kinetic and magnetic) helicities (even though the model itself does not take into account at this stage the helical contributions to evaluate the transport coefficients), we plot in Fig. 4 the time evolution of both kinetic and magnetic helicities, respectively, $H^V(t)$ and $H^M(t)$. Even though both modeled kinetic and magnetic helicities do not exactly match the

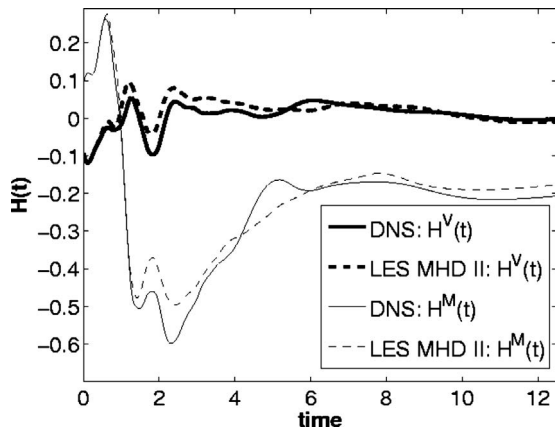


FIG. 4. Time evolution of the kinetic and magnetic helicities for runs I (256^3 DNS) and III (64^3 LES MHD II).

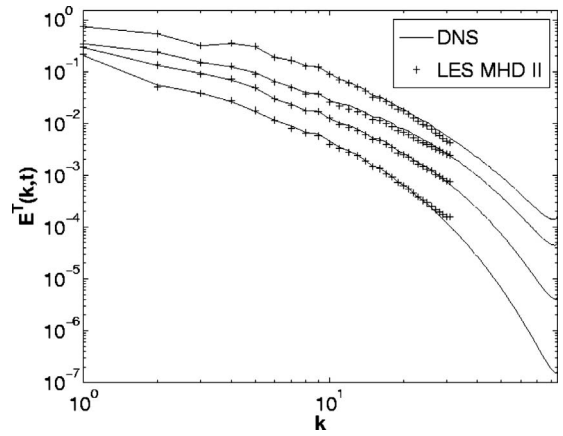


FIG. 5. Total energy spectra $E^T(k)=E^M(k)+E^V(k)$, at time $t=1, 3, 5,$ and 10 , from top to bottom, for runs I (256^3 DNS solid line) and III (64^3 LES MHD II plus signs).

DNS results at each time, they remain close and reproduce the main DNS temporal fluctuations. The LES MHD I model provides similar results (not shown).

We do not present here the temporal evolution of the cross helicity $H^C(t)$, since it is negligible when compared to the total magnetic and kinetic energy. Indeed, this correlation, initially equal to zero, reaches a maximum value of 0.081 for the DNS run, and of 0.069 for the LES MHD II run, to finish, respectively, at values of 0.051 and 0.056.

We now investigate the spectral behavior of our LES model by comparing the DNS and LES MHD II kinetic and magnetic energy spectra at various times. Figure 5 shows the total (kinetic plus magnetic) energy spectra $E^T(k)=E^M(k)+E^V(k)$ at times $t=1, 3, 5,$ and 10 obtained from DNS and LES MHD II computations. At any wave number and at any time, our LES MHD II model reproduces more correctly the DNS spectra than does the LES MHD I model (see Fig. 1). It is clear that the spectral overestimations at small scales obtained with this latter model is cured by the new formulation of the eddy damping rates.

VII. RANDOM FLOW AT $P_M=0.1$

Since the eddy damping times involved in our LES MHD II model allow for a more refined differentiation between the dynamical effects of the magnetic diffusivity and kinematic viscosity, we simulated a flow at a magnetic Prandtl number less than unity, namely, $P_M=0.1$. In order to highlight the efficiency of the damping times in reproducing the flow dynamics, we compared both LES MHD I and II data against DNS results. For these simulations, we kept the initial conditions identical to those of the previous section. A first comparison between the time evolution of the kinetic and magnetic energies computed from a DNS and LES MHD II data is plotted in Fig. 6.

One can observe that the model nearly reproduces the exact temporal evolution of both kinetic and magnetic energies. The evolution of the kinetic and magnetic helicities (not shown) is also well reproduced by the model. Once again, the cross helicity remains weak throughout the simulations.

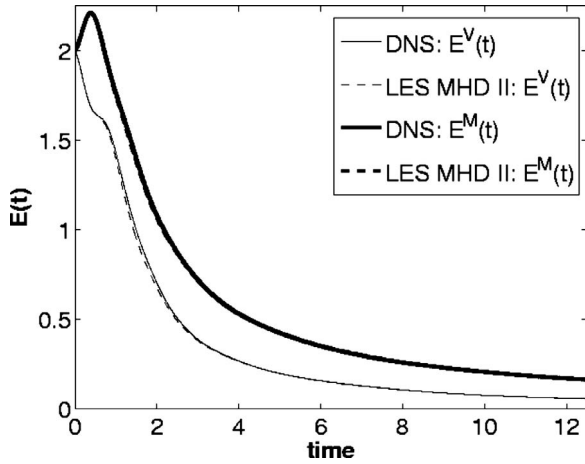


FIG. 6. Total kinetic and magnetic energy temporal evolutions, for runs IV (256^3 DNS), and V (64^3 LES MHD II) at a magnetic Prandtl number of 0.1.

Initially equal to zero, it reaches a maximum value of 0.056 for the DNS, 0.057 for the LES MHD I, and 0.057 for the LES MHD II runs, before it ends with final values of 0.044 (DNS), 0.046 (LES MHD I), and 0.045 (LES MHD II).

In Fig. 7 the total (kinetic plus magnetic) energy spectra evolution are shown at times $t=1, 3, 5,$ and 10 , obtained from DNS, LES MHD I, and LES MHD II data.

Although at small wave numbers, both LES models correctly reproduce the DNS spectra, strong differences appear among these various spectra at large wave numbers. Indeed, the LES MHD II results slightly underestimate this range of DNS spectra, whereas the LES MHD I highly overestimates it.

VIII. DETERMINISTIC ORSZAG-TANG FLOW AT $P_M=1$

For a majority of flows, the cross correlation between the velocity and the magnetic fields (or cross helicity) is non-negligible, leading to a slowing down of the dynamics and to

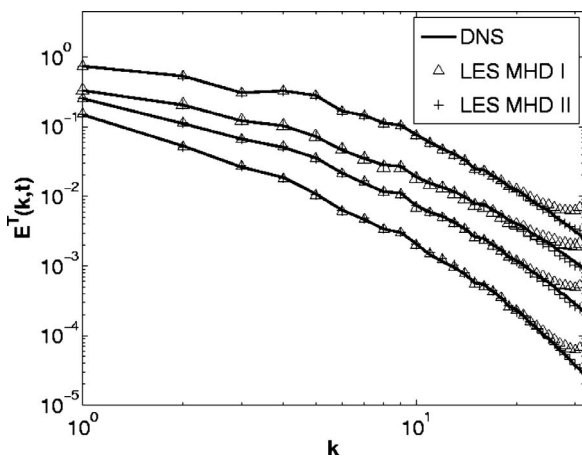


FIG. 7. Total energy spectra, at times $t=1, 3, 5,$ and 10 , from top to bottom, for runs IV (256^3 DNS, solid line), V (64^3 LES MHD II, plus signs), and VI (64^3 LES MHD I, triangles) at $P_M=0.1$.

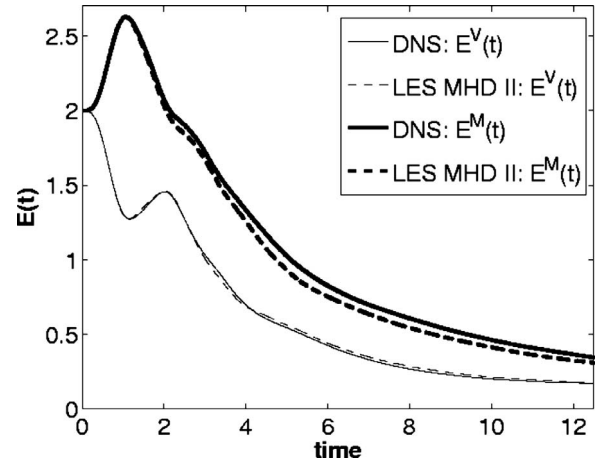


FIG. 8. Kinetic and magnetic energy evolution, for runs VII (256^3 DNS, solid line), and VIII (64^3 LES MHD II, dashed line) with nonzero velocity-magnetic field correlation.

an energy spectra dependence on the amount of the flow correlation [34]. It has also been observed that local patches of either aligned or antialigned velocity-magnetic field configurations can be found both in the solar wind and in numerical simulations [31,32]. We therefore decided to evaluate the ability of our model to simulate flows with strong cross helicity by examining the evolution of the so-called three-dimensional Orszag-Tang flow [with $\mathbf{x}, \mathbf{y},$ and \mathbf{z} the unit vectors in the (x, y, z) directions]:

$$\mathbf{v}(t=0) = -2 \sin(y)\mathbf{x} + 2 \sin(x)\mathbf{y},$$

$$\begin{aligned} \mathbf{b}(t=0) = & [-2 \sin(2y) + \sin(z)]\mathbf{x} + [2 \sin(x) + \sin(z)]\mathbf{y} \\ & + [2 \sin(x) + \sin(y)]\mathbf{z} \end{aligned} \quad (24)$$

with an initial global correlation $H^C(t=0)=1.63$, to be compared with the total kinetic and magnetic energy $E^V(t=0)=E^M(t=0)=2$.

A. Global norms

The kinetic energy obtained from the LES MHD II data fits with great accuracy the DNS kinetic energy (see Fig. 8). However, the magnetic energy, which is well reproduced up to $t=2$, measurably departs from the DNS data after this time.

The global cross helicities, computed from either DNS or LES MHD II data, are quite close (see Fig. 9), demonstrating that, although the model does not explicitly take this quantity into account, it still maintains a reliable evolution for it. However, the well-known temporal growth of the normalized cross-correlation coefficient $\rho(t)=H^C(t)/[E^V(t)+E^M(t)]$ shown in Fig. 10 is not represented as accurately as either E^T or H^C . This could be tentatively attributed to the fact that turbulent transport coefficients based on the velocity-magnetic field correlation itself would emerge from a complete model (as derived in [1]; see also [33]), the effect of which might be to dampen the correlation growth over time.

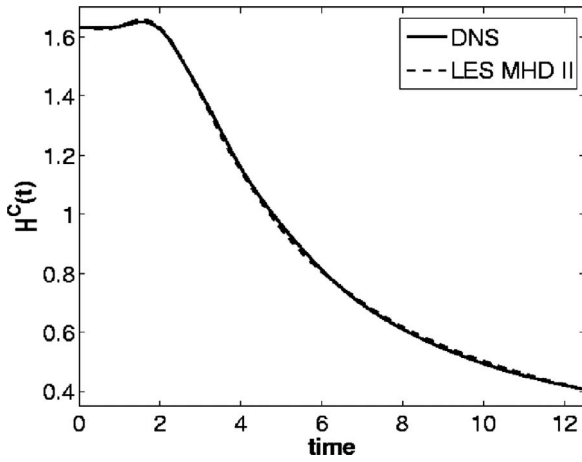


FIG. 9. Global velocity-magnetic field cross helicity, for runs VII (256^3 DNS, solid line), and VIII (64^3 LES MHD II, dashed line).

Note that this discrepancy likely emerges from the less accurate representation of the magnetic energy itself, as displayed in Fig. 8.

B. Spectral features

We investigate finally the spectral behavior of our model for the particular Orszag-Tang flow under study. We, respectively, plot in Figs. 11 and 12 the kinetic and magnetic spectra of both DNS and LES MHD II data, at times $t=1, 3, 5,$ and 10 .

Strong similarities are observed between the modeled and the DNS spectra, although small differences appear at large scales. There may be some fluctuations in the spectra that could be erased by a temporal averaging in the case of stationary flows in the presence of a forcing term; on the other hand, these discrepancies did not appear in the uncorrelated cases of the preceding sections, showing again that the amount of cross helicity is an essential factor in understanding the detailed dynamics of MHD flows; the improvement

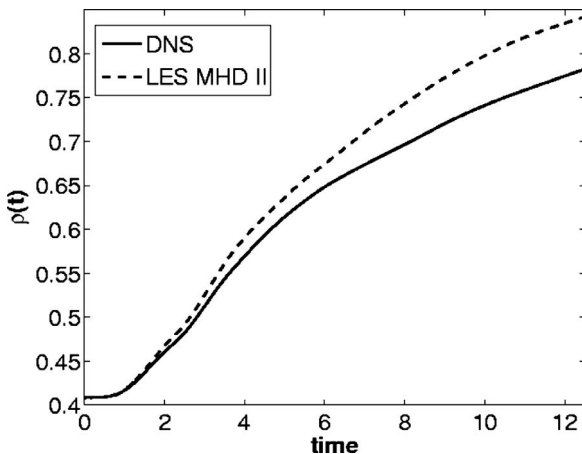


FIG. 10. Correlation coefficient $\rho(t)$, for runs VII (256^3 DNS, solid line), and VIII (64^3 LES MHD II, dashed line).

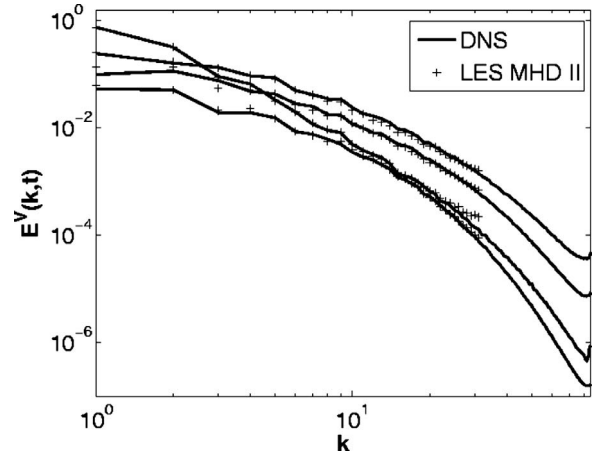


FIG. 11. Kinetic energy spectra, at times $t=1$ (top), 3, 5, and 10 (bottom), for data VII (256^3 DNS, solid line) and VIII (64^3 LES MHD II, plus signs).

needed in the modeling effort in such a case is left for future work.

In order to evaluate the effect of the model on the cross helicity, scale by scale, we represent in Fig. 13 its associated spectra at times $t=3$ and 10 (only two times are shown for a readable plot). At the large scales which are the most energetic, the model correctly reproduces, at both times, the spectra obtained from the DNS data. However, close to the cutoff wave number, the model strongly underestimates the cross helicity. This phenomenon, as stated before, is linked to the eddy viscosity and eddy diffusivity, which dissipate the kinetic and magnetic resolved scales, as well as the cross correlation at these scales. The reconstruction procedure allows energy and helicity (when taken into account) to be reinjected at these scales, but not the cross correlation, since transport coefficients and time scales associated with cross helicity have been left out in the present work, for simplicity.

IX. CONCLUSION

In this paper, we carry out two complementary studies. We first develop a large-eddy simulation spectral model for MHD turbulent flows using the EDQNM equations and

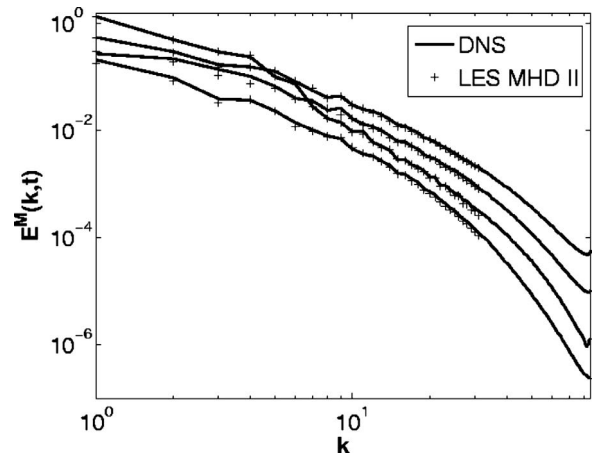


FIG. 12. Magnetic energy spectra for the same runs and times as in Fig. 11.

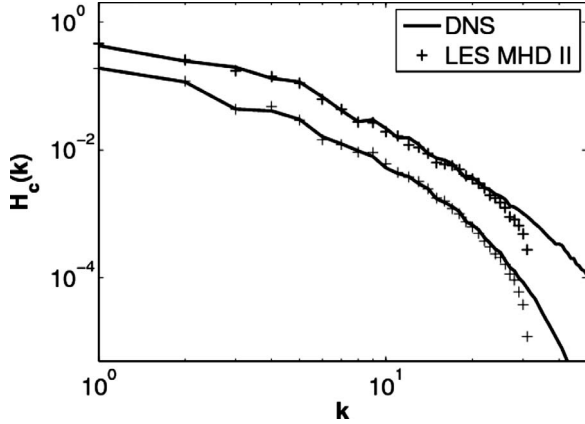


FIG. 13. Cross helicity spectra at $t=3$ (top) and 10 (bottom), for runs VII (256^3 DNS, solid line), and VIII (64^3 LES MHD II, plus signs).

transport coefficients derived in [25], but in the nonhelical case. We then show that not all relevant time scales appearing in the cumulant expansions of the primitive MHD equations are taken into account in the phenomenological formulation of [25]. Indeed, one can derive several new eddy damping times for the EDQNM equations, and document how, by using them, one can considerably improve the treatment of the magnetic and kinetic energy transfers in the LES approach taken in this paper, as shown on three specific examples, at magnetic Prandtl numbers equal to 1 and 0.1, and in the presence or absence of velocity-magnetic field correlations.

Several extensions of this work are possible. One is to incorporate the effect of either cross helicity [33] or kinetic and magnetic helicities [25] in the evaluation of the eddy viscosities and eddy noise derived here. The fact that the modeling algorithm we propose does not depend on a specified inertial index may also be of some help in the case of high velocity-magnetic field correlations when different spectra emerge at high values of the (normalized) H^C cross helicity [34].

The issue of energy spectra in MHD turbulence, still much debated today, may be another possible application of the model presented in this paper. One issue that will be worth checking in this context is to what extent the model does follow the exact laws that can be derived in MHD (under the hypotheses of isotropy, homogeneity, incompressibility, stationnarity, and high Reynolds number) and that stem from energy and cross-helicity conservation [35] (as well as for the other quadratic invariant of the ideal case, e.g., magnetic helicity [36] in the three-dimensional case).

Furthermore, with such a model, many astrophysical and geophysical flows can be studied, and perhaps more importantly a large range of physical parameters, in particular the magnetic Prandtl number, can be examined. Among such problems, the generation of magnetic fields at either low or high magnetic Prandtl number is of prime importance, in particular in the former case in view of a set of laboratory experiments designed to study the dynamo instability in liquid metals [37].

ACKNOWLEDGMENTS

This work is supported by INSU/PNST and PCMI Programs and CNRS/GdR Dynamo. Computation time was provided by IDRIS (CNRS) Grant No. 070597, and SIGAMM mesocenter (OCA/University Nice-Sophia). NCAR is sponsored by NSF.

APPENDIX: EDQNM CLOSURE

For completeness, we recall here the EDQNM closure equations for magnetic and kinetic energies without helicity. The nonhelical EDQNM equations were first derived in [24] but we follow here the notation used in [25], which gives the following closure in the absence of helicity:

$$(\partial_t + 2\nu k^2)E^V(k,t) = \hat{T}^V(k,t), \quad (\text{A1})$$

$$(\partial_t + 2\eta k^2)E^M(k,t) = \hat{T}^M(k,t), \quad (\text{A2})$$

where the nonlinear transfer terms for the kinetic and magnetic energy, respectively, $\hat{T}^V(k,t)$ and $\hat{T}^M(k,t)$, are expressed as

$$\hat{T}^V(k,t) = \int \int_{\Delta_k} (\theta_{kpq}^{VV} S^{VV} + \theta_{kpq}^{VM} S^{VM}) dp dq, \quad (\text{A3})$$

$$\hat{T}^M(k,t) = \int \int_{\Delta_k} (\theta_{kpq}^{MM} S^{MM} + \theta_{kpq}^{MV} S^{MV}) dp dq. \quad (\text{A4})$$

Here Δ_k is the integration domain over \mathbf{p} and \mathbf{q} , such that $(\mathbf{k}, \mathbf{p}, \mathbf{q})$ form a triangle. In the formulation derived in Pouquet *et al.* [25], the θ 's, called triad relaxation times, are unique and read

$$\theta_{kpq}(t) = \theta_{kpq}^{VV} = \theta_{kpq}^{VM} = \theta_{kpq}^{MV} = \theta_{kpq}^{MM} = \frac{1 - e^{-\mu_{kpq}t}}{\mu_{kpq}}, \quad (\text{A5})$$

with $\mu_{kpq} = \mu_k + \mu_p + \mu_q$ where the μ_k 's are called eddy damping rates and read

$$\begin{aligned} \mu_k = & + \lambda \left(\int_0^k q^2 (E_q^V + E_q^M) dq \right)^{1/2} \\ & + \sqrt{\frac{2}{3}} k \left(\int_0^k E_q^M dq \right)^{1/2} + (\nu + \eta) k^2. \end{aligned} \quad (\text{A6})$$

The constant λ can be expressed as a function of the Kolmogorov constant C_k appearing in front of the kinetic energy spectrum such that

$$\lambda = 0.218 C_k^{3/2}, \quad (\text{A7})$$

following [22].

The only difference between this classical EDQNM closure for MHD and the new formulation we develop here resides in the introduction of triad relaxation times; they read

$$\theta_{kpq}^{XY}(t) = \frac{1 - e^{-\mu_{kpq}^{XY}t}}{\mu_{kpq}^{XY}}, \quad (\text{A8})$$

with $\mu_{kpq}^{XY} = \mu_k^{XY} + \mu_p^{XY} + \mu_q^{XY}$ and with XY standing for VV , VM , MV , or MM and with

$$\mu_k^{VV} = [\tau_D^{VV}(k)]^{-1} + [\tau_{NL}(k)]^{-1}, \quad (\text{A9})$$

$$\mu_k^{VM} = [\tau_D^{VM}(k)]^{-1} + [\tau_{NL}(k)]^{-1} + [\tilde{\tau}_A(k)]^{-1}, \quad (\text{A10})$$

$$\mu_k^{MV} = [\tau_D^{MV}(k)]^{-1} + [\tau_{NL}(k)]^{-1} + [\tilde{\tau}_A(k)]^{-1}, \quad (\text{A11})$$

$$\mu_k^{MM} = [\tau_D^{MM}(k)]^{-1} + [\tau_{NL}(k)]^{-1} + [\tilde{\tau}_A(k)]^{-1}, \quad (\text{A12})$$

where the different characteristic times are defined in Sec. IV.

The S^{VV} , S^{VM} , S^{MV} , and S^{MM} terms can be further expanded as

$$\begin{aligned} S^{VV} &= \frac{k}{pq} b_{kpq} [k^2 E^V(q,t) E^V(p,t) - p^2 E^V(q,t) E^V(k,t)] \\ &= S_1^V(k,p,q,t) + S_2^V(k,p,q,t), \end{aligned} \quad (\text{A13})$$

$$\begin{aligned} S^{VM} &= \frac{k}{pq} c_{kpq} [k^2 E^M(q,t) E^M(p,t) - p^2 E^M(q,t) E^V(k,t)] \\ &+ S_3^V(k,p,q,t) + S_4^V(k,p,q,t), \end{aligned} \quad (\text{A14})$$

$$\begin{aligned} S^{MV} &= \frac{k}{pq} h_{kpq} [k^2 E^M(p,t) E^V(q,t) - p^2 E^V(q,t) E^M(k,t)] \\ &= S_1^M(k,p,q,t) + S_2^M(k,p,q,t), \end{aligned} \quad (\text{A15})$$

$$\begin{aligned} S^{MM} &= \frac{k^3}{pq} c_{kpq} \left(\frac{k^2}{p^2} E^V(p,t) E^M(q,t) - E^M(q,t) E^M(k,t) \right) \\ &+ S_3^M(k,p,q,t) + S_4^M(k,p,q,t). \end{aligned} \quad (\text{A16})$$

In Eqs. (A14) and (A16) the geometric coefficients b_{kpq} , c_{kpq} , and h_{kpq} are defined as

$$b_{kpq} = pk^{-1}(xy + z^3), \quad c_{kpq} = pk^{-1}z(1 - y^2),$$

$$h_{kpq} = z(1 - y^2),$$

where x , y , and z are the cosines of the interior angles opposite to \mathbf{k} , \mathbf{p} , and \mathbf{q} . This completes the description of the EDQNM closure for MHD as developed in [24,25]. The helical case, dealt with in [28] for a pure (neutral) fluid and in [25] from the EDQNM standpoint, will be studied in a forthcoming presentation.

-
- [1] R. Grappin, J. Léorat and A. Pouquet, *Astron. Astrophys.* **123**, 51 (1983).
- [2] W. H. Matthaeus and M. L. Goldstein, *J. Geophys. Res.* **87**, 6011 (1982).
- [3] P. Iroshnikov, *Sov. Astron.* **7**, 566 (1963); R. H. Kraichnan *Phys. Fluids* **8**, 1385 (1965).
- [4] J. Maron and P. Goldreich, *Astrophys. J.* **554**, 1175 (2001).
- [5] W. C. Müller and R. Grappin, *Phys. Rev. Lett.* **95**, 114502 (2005).
- [6] P. D. Mininni and A. Pouquet, *Phys. Rev. Lett.* **99**, 254502 (2007).
- [7] J. Podesta, D. Roberts, and M. Goldstein, *Astrophys. J.* **664**, 543 (2007).
- [8] K. Yoshida and T. Arimitsu *Phys. Fluids* **19**, 045106 (2007).
- [9] S. Galtier, S. Nazarenko, A. C. Newell, and A. Pouquet, *J. Plasma Phys.* **63**, 447 (2000); *Astrophys. J. Lett.* **564**, L49 (2002).
- [10] J. Saur, H. Politano, A. Pouquet, and W. Matthaeus, *Astron. Astrophys.* **386**, 699 (2002).
- [11] *Magnetohydrodynamics* **38**, (2002), special issue on MHD dynamo experiments, edited by A. Cebers and K. H. Rädler.
- [12] N. L. Peffley, A. B. Cawthorne, and D. P. Lathrop, *Phys. Rev. E* **61**, 5287 (2000).
- [13] M. Bourgoïn, L. Marie, F. Pétrélis, C. Gasquet, A. Guigon, J. B. Luciani, M. Moulin, J. Namer, A. Burguete, Chiffaudel, F. Daviaud, S. Fauve, P. Odier, and J.-F. Pinton, *Phys. Fluids* **14**, 3046 (2002).
- [14] F. Pétrélis, M. Bourgoïn, L. Marié, J. Burguete, A. Chiffaudel, F. Daviaud, S. Fauve, P. Odier, and J.-F. Pinton, *Phys. Rev. Lett.* **90**, 174501 (2003).
- [15] Y. Ponty, H. Politano, and J. F. Pinton, *Phys. Rev. Lett.* **92**, 144503 (2004).
- [16] Y. Ponty, P. D. Mininni, D. C. Montgomery, J.-F. Pinton, H. Politano, and A. Pouquet, *Phys. Rev. Lett.* **94**, 164502 (2005).
- [17] A. Alexakis, P. D. Mininni, and A. Pouquet, *Phys. Rev. E* **72**, 046301 (2005).
- [18] P. D. Mininni, A. Alexakis, and A. Pouquet, *Phys. Rev. E* **72**, 046302 (2005).
- [19] O. Debligny, M. K. Verma, and D. Carati, *Phys. Plasmas* **12**, 042309 (2005).
- [20] O. Agullo, W. C. Muller, B. Knaepen, and D. Carati, *Phys. Plasmas* **8**, 3502 (2001).
- [21] P. Mininni, A. Pouquet, and P. Sullivan, in *Proceedings of the Summer School on Mathematics in Geophysics*, edited by Roger Temam and Joe Tribbia (Springer-Verlag, Berlin, in press).
- [22] J.-P. Chollet and M. Lesieur, *J. Atmos. Sci.* **38**, 2747 (1981).
- [23] A. Pouquet, *Magnetohydrodynamic Turbulence*, edited by J. P. Zahn and J. Zinn-Justin, Proceedings of the Les Houches Summer School of Theoretical Physics XLVII (Elsevier, Amsterdam, 1993), p. 139.
- [24] R. H. Kraichnan and S. Nagarajan, *Phys. Fluids* **10**, 859 (1967).
- [25] A. Pouquet, U. Frisch, and J. Léorat, *J. Fluid Mech.* **77**, 321 (1976).
- [26] E. Parker, *Cosmical Magnetic Fields: Their Origin and Their Activity* (Oxford University Press, New York, 1979).
- [27] H. K. Moffatt, *Magnetic Field Generation in Electrically Conducting Fluids* (Cambridge University Press, Cambridge, U.K., 1978).
- [28] J. Baerenzung, H. Politano, Y. Ponty, and A. Pouquet, *Phys. Rev. E* **77**, 046303 (2008).
- [29] J. Baerenzung, Ph.D. thesis, Université de Nice-Sophia Antipolis, Observatoire de la Côte d'Azur, 2008.
- [30] J. D. Fournier, P. L. Sulem, and A. Pouquet, *J. Phys. A* **15**, 1393 (1982).

- [31] M. Meneguzzi, H. Politano, A. Pouquet, and M. Zolver, *J. Comput. Phys.* **123**, 32 (1996).
- [32] W. H. Matthaeus, A. Pouquet, P. D. Mininni, P. Dmitruk, and B. Breech, *Phys. Rev. Lett.* **100**, 085003 (2008).
- [33] R. Grappin, U. Frisch, J. Léorat, and A. Pouquet, *Astron. Astrophys.* **105**, 6 (1982).
- [34] A. Pouquet, P. L. Sulem, and M. Meneguzzi *Phys. Fluids* **31**, 2635 (1988).
- [35] H. Politano and A. Pouquet, *Geophys. Res. Lett.* **25**, 273 (1998).
- [36] H. Politano, T. Gomez, and A. Pouquet, *Phys. Rev. E* **68**, 026315 (2003).
- [37] R. Monchaux, M. Berhanu, M. Bourgoïn, M. Moulin, P. Odier, J.-F. Pinton, R. Volk, S. Fauve, N. Mordant, F. Pétrélis, A. Chiffaudel, F. Daviaud, B. Dubrulle, C. Gasquet, L. Marié, and F. Ravelet, *Phys. Rev. Lett.* **98**, 044502 (2007).